

LatentSync: Taming Audio-Conditioned Latent Diffusion Models for Lip Sync with SyncNet Supervision

Chunyu Li^{1,2} Chao Zhang¹ Weikai Xu¹ Jingyu Lin³ Jinghui Xie^{1,†}
 Weiguo Feng¹ Bingyue Peng¹ Cunjian Chen³ Weiwei Xing^{2,†}
¹ByteDance ²Beijing Jiaotong University ³Monash University

Abstract

End-to-end audio-conditioned latent diffusion models (LDMs) have been widely adopted for audio-driven portrait animation, demonstrating their effectiveness in generating lifelike and high-resolution talking videos. However, direct application of audio-conditioned LDMs to lip-synchronization (lip-sync) tasks results in suboptimal lip-sync accuracy. Through an in-depth analysis, we identified the underlying cause as the “shortcut learning problem”, wherein the model predominantly learns visual-visual shortcuts while neglecting the critical audio-visual correlations. To address this issue, we explored different approaches for integrating SyncNet supervision into audio-conditioned LDMs to explicitly enforce the learning of audio-visual correlations. Since the performance of SyncNet directly influences the lip-sync accuracy of the supervised model, the training of a well-converged SyncNet becomes crucial. We conducted the first comprehensive empirical studies to identify key factors affecting SyncNet convergence. Based on our analysis, we introduce *StableSyncNet*, with an architecture designed for stable convergence. Our *StableSyncNet* achieved a significant improvement in accuracy, increasing from 91% to 94% on the *HDTF* test set. Additionally, we introduce a novel *Temporal Representation Alignment (TREPA)* mechanism to enhance temporal consistency in the generated videos. Experimental results show that our method surpasses state-of-the-art lip-sync approaches across various evaluation metrics on the *HDTF* and *VoxCeleb2* datasets. Code and models are publicly available at <https://github.com/bytedance/LatentSync>.

1. Introduction

The lip sync [14, 28, 29, 52] is a video editing task, which regenerates the lip movements of a talking person according to the given audio, while maintaining the head pose and personal identity. This technique has broad applications in

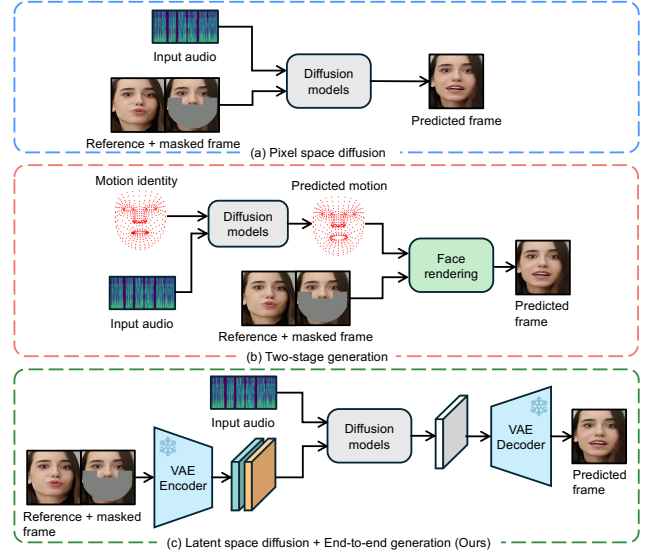


Figure 1. Frameworks comparison between previous diffusion-based lip-sync methods and our method.

numerous practical domains, such as visual dubbing, virtual avatars, and video conferencing.

In the field of lip sync, GAN-based methods [14, 29] remain the mainstream approaches. The main issue with these methods is that they struggle to scale up [21, 36] to large and diverse datasets due to the unstable training [2, 35] and mode collapse [6, 39]. Recent studies proposed diffusion-based methods [3, 25, 28, 48, 53] for lip sync, allowing the model to easily generalize across different individuals without the need for further fine-tuning on specific identities. However, these methods still have some limitations. Specifically, [3, 28] perform the diffusion process in the pixel space (Fig. 1 a), which restricts its ability to generate high-resolution videos due to the prohibitive hardware requirements. Other methods [48, 53] adopt a two-stage approach: the first stage generates lip motions from audio, and the second stage synthesizes the visual appearance conditioned on the motion (Fig. 1 b). The issue with this two-stage ap-

proach is that subtly different sounds may map to the same motion representation, leading to the loss of nuanced expressions linked to the emotional tone of the speech.

To address the above limitations, we propose *LatentSync*, an end-to-end lip sync framework based on audio-conditioned LDMs [33] to generate lifelike and high-resolution talking videos, as shown in Fig. 1 (c). We initially tried directly applying methods from the field of audio-driven portrait animation, such as EMO [41] and Hallo [46]. However, the results showed poor lip-sync accuracy. We delved deeper into this phenomenon and identified the “shortcut learning problem” [12] inherent in lip sync task.

The shortcut learning problem in lip sync. Lip-sync methods are typically based on a video-to-video inpainting framework, the model receives masked frames and audio as inputs. Unexpectedly, the audio-conditioned LDMs tends to predict lip movements based on visual information around the lips, such as facial muscles, eyes, and cheeks, while ignoring the audio information. We conducted an experiment to validate the existence of the shortcut learning problem and the effectiveness of SyncNet supervision [29] in mitigating this issue. We trained the audio-conditioned LDMs with masks of different sizes, both with and without SyncNet supervision. We used the sync confidence score [9] to evaluate the synchronization accuracy between audio and lip movements.





Masks of different sizes				
w/o SyncNet supervision	2.5	4.3	4.6	6.7
w/ SyncNet supervision	8.3	8.6	8.9	9.1

Figure 2. The shortcut learning problem in the lip-sync task. Higher sync confidence score means better lip-sync accuracy.

As shown in Fig. 2, without SyncNet supervision, as the mask size increases, the visual information available in the masked frame for inferring lip movements decreases, forcing the model to rely more on audio information, thereby improving lip-sync accuracy, and vice versa. In contrast, with SyncNet supervision, the model remains focused on learning audio-visual correlations across different mask sizes.

Why is SyncNet supervision not necessary for audio-driven portrait animation methods? These methods [7, 20, 41, 46] are based on image-to-video framework. Since they do not involve input masked frames, they do not suffer from the shortcut learning problem.

The previous work Diff2Lip [28] has explored how to add SyncNet supervision to pixel-space diffusion models. However, how to effectively apply SyncNet to latent diffu-

sion models [33] remains unclear. Specifically, we explored two methods to incorporate SyncNet supervision into latent diffusion models: (a) Decoded pixel space supervision and (b) Latent space supervision. Furthermore, We found that SyncNet struggles to converge in both latent space and high-resolution pixel space. Since the convergence of SyncNet significantly impacts its supervision effectiveness, and ultimately affects the lip-sync accuracy of the supervised model, the convergence issue of SyncNet is highly valuable for research. Therefore, we conducted the first comprehensive empirical studies in the aspects of model architecture design, training hyperparameters, and data preprocessing techniques, introducing the StableSyncNet with an architecture designed for stable convergence. Our StableSyncNet achieved the unprecedented 94% accuracy on HDTF [51].

Additionally, we observed that high-frequency details in the generated talking videos, such as teeth, lips, and facial hair, exhibit flickering artifacts. We propose TREPA, a novel method designed to enhance temporal consistency and reduce such artifacts.

In summary, we made the following contributions: (1) We proposed LatentSync, the first lip-sync method that utilizes audio-conditioned LDMs to achieve end-to-end lifelike lip sync on high-resolution videos, incorporating TREPA to enhance the temporal consistency in the generated videos. (2) We identified the shortcut learning problem in lip-sync task and explored different methods to incorporate SyncNet supervision into audio-conditioned LDMs. (3) We conducted the first comprehensive empirical studies to identify key factors affecting SyncNet convergence, introducing the StableSyncNet for stable convergence.

2. Related Work

2.1. Diffusion-based Lip Sync

Diff2Lip [28] and DrivenVideoEditing [3] are both end-to-end lip sync methods based on pixel-space audio-conditioned diffusion models. MyTalk [48] uses diffusion models in the first stage to complete audio-to-motion conversion and uses a VAE [23] in the second stage for motion-to-image generation. StyleSync [53] uses transformers in the first stage to convert audio to motion and employs diffusion models in the second stage for motion-to-image generation. DiffDub [25] uses diffusion autoencoders [30] to convert the masked images into semantic latent codes in the first stage, and uses diffusion models to generate an image conditioned on the semantic latent codes and audio in the second stage.

2.2. Non-diffusion-based Lip Sync

Wav2Lip [29] is the most classic lip sync method that introduced using a pretrained SyncNet [9] to supervise the training of the lip-sync generator. [16] trains a VQ-VAE [11] to

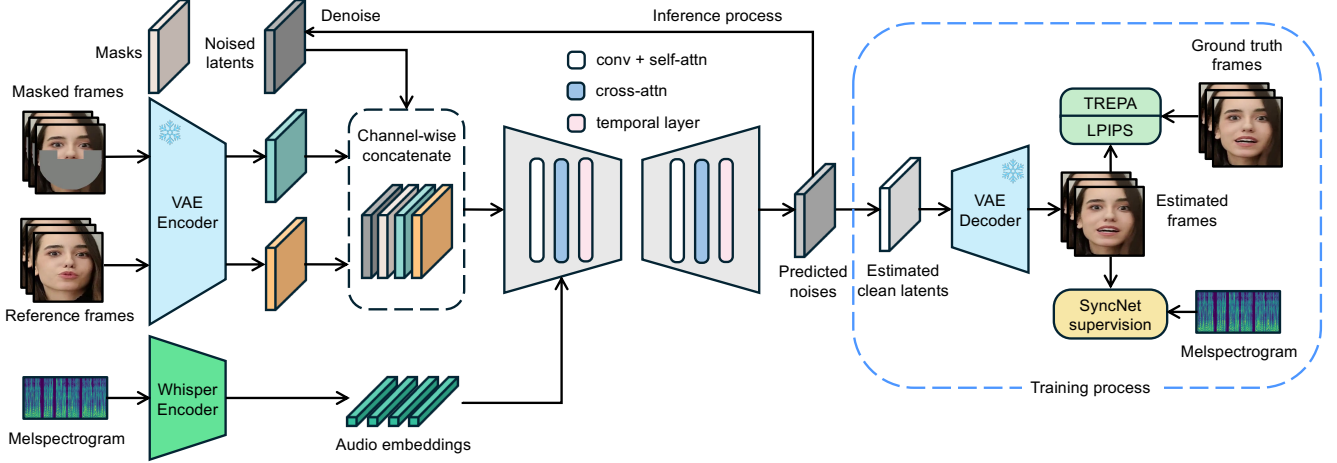


Figure 3. The overview of our LatentSync framework. We use the Whisper [32] to convert melspectrogram into audio embeddings, which are then integrated into the U-Net [34] via cross-attention layers. The reference and masked frames are channel-wise concatenated with noised latents as the input of U-Net. In the training process, we use a one-step method to get estimated clean latents from predicted noises, which are then decoded to obtain the estimated clean frames. The TREPA, LPIPS [49] and SyncNet loss [29] are added in the pixel space.

encode faces and head poses, and then trains the lip sync generator in the quantized space to generate high-resolution images. StyleSync [14] follows the overall framework of Wav2Lip, with its main innovation being the use of StyleGAN2 [22] as the generator backbone. VideoReTalking [8] divides lip sync into three components: semantic-guided reenactment network, lip sync network, and identity-aware refinement and enhancement. DNet [52] deforms the feature maps to generate mouth shapes conditioned on the driving audio. MuseTalk [50] uses the architecture of Stable Diffusion [33] for inpainting, but it does not perform diffusion process and uses a discriminator for adversarial learning [13], making it more like a GAN-based framework.

2.3. Audio-driven Portrait Animation

Many people may confuse lip sync with audio-driven portrait animation. These two tasks have some similarities but are actually completely different tasks. Lip sync is based on video-to-video editing framework, which needs to keep areas other than the mouth the same as in the input video. Audio-driven portrait animation is based on image-to-video animation framework, which can change the head movement and even facial expressions. Although there are already some audio-driven portrait animation methods based on audio-conditioned LDMs, such as [7, 20, 41, 46], they cannot be directly applied to the lip sync task due to the shortcut learning problem.

3. Method

3.1. LatentSync Framework

The overview of the LatentSync framework is shown in Fig. 3. The framework is based on video-to-video inpaint-

ing with the temporal modeling by temporal layer [15]. To incorporate the visual features of the face from the input video, reference frames are introduced as additional inputs. During training, these frames are randomly selected, while during inference, they are taken from the current frames. We concatenate different inputs along the channel dimension, making the total input of U-Net to be 13 channels (4 channels for noise latent, 1 channel for the mask, 4 channels for the masked frame, and 4 channels for the reference frame). At the beginning of training, the model is initialized with the parameters of SD 1.5 [33], except for the first `conv_in` layer with 13 channels and cross-attention layers of dimension 384, which are randomly initialized.

Audio layers. We used the pretrained audio feature extractor Whisper [32] to extract audio embeddings. Lip motion may be influenced by the audio from the surrounding frames, and a larger range of audio input also provides more temporal information for the model. Therefore, for each generated frame, we bundled the audio from several surrounding frames as input. We define the input audio feature $A^{(f)}$ for the f th frame as: $A^{(f)} = \{a^{(f-m)}, \dots, a^{(f)}, \dots, a^{(f+m)}\}$, where m is the number of surrounding audio features from one side. To integrate the audio embeddings into the U-Net [34], we used the native cross-attention layer.

Affine transformation and fixed mask. During the data preprocessing stage, affine transformation was employed to perform face frontalization. This approach [14] helps the model to effectively learn facial features particularly in challenging scenarios such as side-profile views. We applied a mask that covers the entire face to minimize the model’s tendency to learn visual-visual shortcuts. The position and shape of the mask are fixed. We do not use the de-

tected landmarks [5, 26] to draw the mask, as moving landmarks also provide cues about lip movements. The affine transformation and fixed mask are illustrated in Fig. 4.



Figure 4. The illustration of affine transformation and fixed mask.

SyncNet supervision. Latent diffusion models predict in the noise space, while SyncNet [9, 29] requires an input in the image space. To address this issue, we use the predicted noise $\epsilon_\theta(z_t)$ to obtain the estimated \hat{z}_0 in one step, which can be formulated as:

$$\hat{z}_0 = (z_t - \sqrt{1 - \bar{\alpha}_t} \epsilon_\theta(z_t)) / \sqrt{\bar{\alpha}_t} \quad (1)$$

Another problem is that latent diffusion models make predictions in the latent space. We explored two methods to incorporate SyncNet supervision into latent diffusion models: (a) **Decoded pixel space supervision**, which trains SyncNet in the same way as Wav2Lip [29]. (b) **Latent space supervision**, which requires training a SyncNet in the latent space. The visual encoder input of this SyncNet is the latent vectors obtained by the VAE [11, 23] encoding. The illustration is shown in Fig. 5. Our empirical analysis in Sec. 5.3 reveals that training SyncNet in the latent space exhibits inferior convergence compared to training in the pixel space. This degradation may arise from information loss in the lip region during the VAE encoding process. The poorer convergence of SyncNet in the latent space adversely impacts the lip-sync accuracy of the supervised diffusion models, according to the experimental results in Sec. 5.3. Therefore, we finally choose the decoded pixel space supervision in the LatentSync framework.

3.2. Two-Stage Training Strategy

The decoded pixel space supervision has a problem that the activations in VAE decoding need to be stored for backpropagation, which significantly increases GPU memory consumption. To mitigate this issue, we designed a two-stage training strategy: in the first stage, the model learns to extract features from reference frames and develops inpainting capabilities, which we refer to as learning visual features. In the second stage, it learns audio-visual correlations under SyncNet supervision. This approach eliminates the need for the VAE decoding process in the first stage, enabling model to learn visual features with a larger batch size. We observed that audio-conditioned LDMs typically spend more time learning visual features and less time learning audio-visual correlations. Therefore, this two-stage training strategy allows the model to efficiently learn both visual features

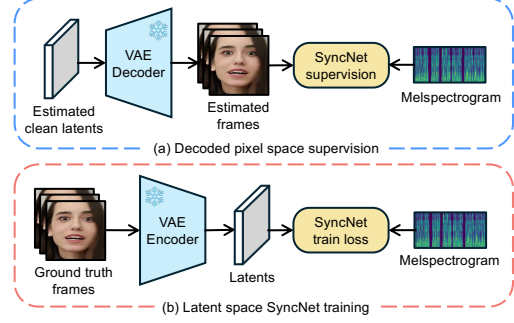


Figure 5. Two methods to add SyncNet supervision to latent diffusion models.

and audio-visual correlations. We provide the formal definitions of training objectives in the following paragraphs.

In the first stage of training, we do not add the temporal layer [4, 15] and train all parameters of the U-Net. The training objective has only a simple loss [19]:

$$\mathcal{L}_{\text{simple}} = \mathbb{E}_{x,A,\epsilon \sim \mathcal{N}(0,1),t} [\|\epsilon - \epsilon_\theta(z_t, t, \tau_\theta(A))\|_2^2] \quad (2)$$

where A is the input audio, $\epsilon_\theta(z_t, t, \tau_\theta(A))$ is the predicted noise, and τ_θ is the audio feature extractor.

In the second stage of training, we only train the temporal layer and audio layer while freezing the other parameters of the U-Net. Suppose we have 16 decoded video frames $\mathcal{D}(\hat{z}_0)_{f:f+16}$ and the corresponding audio sequence $a_{f:f+16}$, the SyncNet loss can be formulated as:

$$\mathcal{L}_{\text{sync}} = \mathbb{E}_{x,a,\epsilon,t} [\text{SyncNet}(\mathcal{D}(\hat{z}_0)_{f:f+16}, a_{f:f+16})] \quad (3)$$

where \mathcal{D} represents the VAE decoder, since the lipsync task requires generating detailed areas, such as lips, teeth, and facial hair, we used the LPIPS [49] to improve the visual quality of the images generated by the U-Net.

$$\mathcal{L}_{\text{lipps}} = \mathbb{E}_{x,\epsilon,t} [\|\mathcal{V}_l(\mathcal{D}(\hat{z}_0)_f) - \mathcal{V}_l(x_f)\|_2^2] \quad (4)$$

where $\mathcal{V}_l(\cdot)$ denotes the features extracted from the l^{th} layer of a pretrained VGG network [37]. In addition, to improve temporal consistency, we also employed the proposed TREPA, see Eq. (6). For more details of the TREPA, please refer to Sec. 3.3.

The total loss function for the second stage of training is:

$$\mathcal{L}_{\text{total}} = \lambda_1 \mathcal{L}_{\text{simple}} + \lambda_2 \mathcal{L}_{\text{sync}} + \lambda_3 \mathcal{L}_{\text{lipps}} + \lambda_4 \mathcal{L}_{\text{trepa}} \quad (5)$$

3.3. Temporal Representation Alignment

TREPA aligns the temporal representations of the generated image sequences with those of ground truth image sequences. The insight behind this method is that merely employing distance loss between individual images improves the content quality of single generated images but does

not enhance the temporal consistency of the generated image sequence. In contrast, temporal representations capture temporal correlation within image sequences, enabling the model to focus on improving the overall temporal consistency. We employed a large-scale self-supervised video model VideoMAE-v2 [44] to extract temporal representations. Due to its unsupervised training on large-scale unlabeled datasets, the model’s temporal representations exhibit strong generalization capabilities, robustness, and high information density.

In mathematical form, let \mathcal{T} be the self-supervised video model encoder. The encoder’s output is the embedding before the head projection. TREPA can be represented as:

$$\mathcal{L}_{\text{trepa}} = \mathbb{E}_{x, \epsilon, t} \left[\|\mathcal{T}(\mathcal{D}(\hat{z}_0)_{f:f+16}) - \mathcal{T}(x_{f:f+16})\|_2^2 \right] \quad (6)$$

where the straightforward Mean Squared Error (MSE) is employed to measure the distance between temporal representations. We also fix the representation by ℓ_2 normalization before calculating the MSE.

4. Empirical Studies on SyncNet Convergence

Our experiments reveal that SyncNet is difficult to converge in both latent space and high-resolution pixel space, a typical characteristic of this issue is that the training loss gets stuck at 0.69 and fails to decrease further. In this section, we analyze the SyncNet convergence problem and identify several critical factors affecting the convergence through various ablation studies. Importantly, we preserved SyncNet’s original training framework and employed the same contrastive loss function as Wav2Lip [29]. Therefore, our experience can be applied to many lip-sync [8, 14, 28, 29, 50, 52] and audio-driven portrait animation methods [27, 47] that utilize SyncNet.

Why is the SyncNet training loss stuck at 0.69? According to the classic training framework of SyncNet [9, 29], we randomly provide SyncNet with positive and negative samples with a 50% probability during the training stage. The output of SyncNet is a probability distribution of whether the sample is positive or negative. We define $p(x = 1)$ as the probability that the sample is positive, and $p(x = 0)$ as the probability that the sample is negative. Let $p(x)$ be the true probability distribution and $q(x)$ the predicted probability distribution. When $q(x = 1) \approx q(x = 0) \approx 0.5$ and batch size N is sufficiently large, the training loss of SyncNet is (proof in Appendix A):

$$\mathcal{L}_{\text{syncnet}} = -\frac{1}{N} \sum_{i=1}^N \sum_{x_i \in \{0,1\}} p(x_i) \log q(x_i) \approx 0.693 \quad (7)$$

This means that SyncNet has not learned any discriminative capability; it is just randomly guessing whether the samples

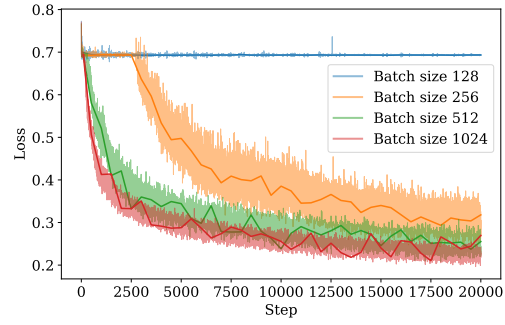


Figure 6. SyncNet training curves of different batch sizes. VoxCeleb2 results, the more transparent curves represent the training set loss, while the darker curves represent the validation set loss; the same applies to the following figures. (VoxCeleb2, Dim 2048, StableSyncNet arch, 16 frames.)

are positive or negative. This may be due to various reasons, including the model’s insufficient capacity to fit the data, the large audio-visual offset in the data, and flaws in the training strategy. In the following paragraphs, we will identify the key factors affecting the convergence of SyncNet through comprehensive ablation studies.

Batch size. As shown in Fig. 6, a larger batch size (e.g., 1024) not only enables the model to converge faster and more stably but also results in a lower validation loss at the end of training. In contrast, smaller batch sizes (e.g., 128) may fail to converge, with the loss remaining stuck at 0.69. Even with a slightly larger batch size (e.g., 256), while convergence may be achieved, the training loss exhibits significant oscillations during its descent.

Architecture. We redesign the SyncNet’s visual and audio encoders with the U-Net encoder from Stable Diffusion 1.5 [33], retaining the structure of residual blocks [17] and self-attention blocks [43] in the U-Net encoder blocks. We only adjusted the downsampling factors based on the size of the input visual images and mel-spectrograms, and we removed the cross-attention blocks, as SyncNet does not require additional conditions. We refer to the SyncNet with this modified architecture as *StableSyncNet*. As shown in Fig. 7, StableSyncNet maintained both training loss and validation loss lower than those of Wav2Lip’s SyncNet [29] throughout the training process.

Embedding dimension. As illustrated in Fig. 8, embeddings with smaller dimensions (e.g., 512) result in representations that fail to capture sufficient semantic information, while larger dimensions (e.g., 4096 or 6144) lead to sparse representations, thereby impeding model convergence. We identified that an optimal embedding dimension of 2048 is suitable for images with an input resolution of 256×256 pixels.

Number of frames. The number of input frames deter-

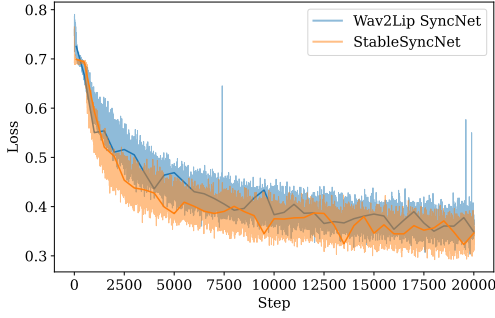


Figure 7. SyncNet training curves of different architectures. For comparison, we also modified the architecture of Wav2Lip’s SyncNet to accept 256×256 visual input according to [31]. (VoxCeleb2, Dim 2048, Batch size 512, 5 frames.)

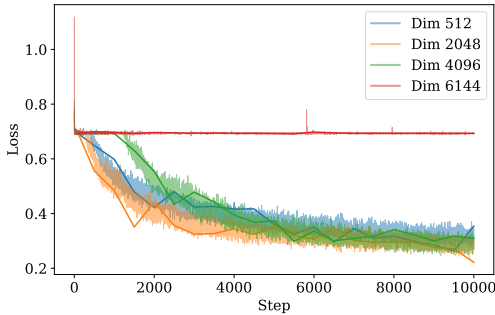


Figure 8. SyncNet training curves of different embedding dimensions. (VoxCeleb2, Batch size 512, StableSyncNet arch, 16 frames.)

mines the range of visual and audio information that SyncNet can perceive. As shown in Fig. 9, selecting a larger number of frames (e.g., 16) can help the model converge. However, an excessively large number of frames (e.g., 25) will cause the model to get stuck around 0.69 in the early stage of training, and the validation loss at the end of training does not show a significant advantage compared to using 16 frames.

Data preprocessing. In-the-wild videos naturally contain audio-visual offsets, it is necessary to adjust this offset to zero before inputting them into the SyncNet network. We used the official open-source version of pretrained SyncNet [9] to adjust the offset and remove videos with $\text{Sync}_{\text{conf}}$ below 3. Specifically, we evaluated adjusting the offset before and after applying affine transformation. As shown in Fig. 10, without offset adjustment, the model’s convergence is significantly impaired. Performing affine transformation before offset adjustment yields better results. This may be due to that affine transformation reducing data with side profiles or unusual angles, allowing the pretrained SyncNet [9] to predict the offset more accurately.

Discussions. Based on the ablation studies above, we found

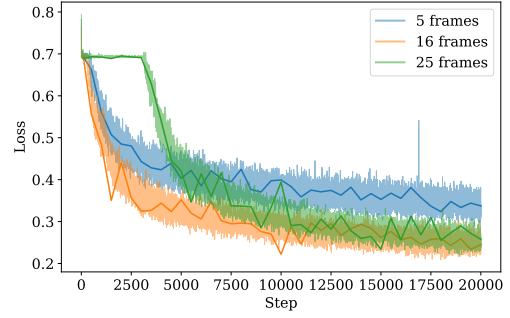


Figure 9. SyncNet training curves of different numbers of input frames. (VoxCeleb2, Batch size 512, StableSyncNet arch, Dim 2048.)

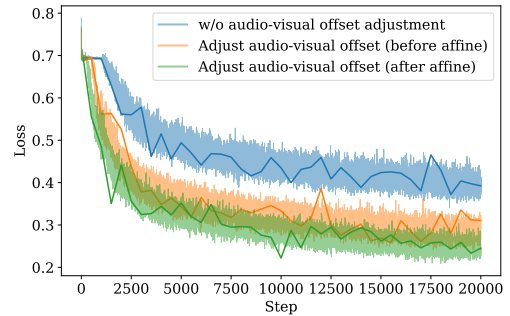


Figure 10. SyncNet training curves of different data preprocessing methods. (VoxCeleb2, Batch size 512, StableSyncNet arch, Dim 2048, 16 frames.)

that batch size, number of input frames, and data preprocessing method are the primary factors affecting SyncNet convergence. We identified the optimal settings for a StableSyncNet with the 256×256 input size: batch size of 1024, 16 frames, SD U-Net encoder adapted for both visual and audio encoders, embedding dimension of 2048, and adjusting the audio-visual offset after affine transformation. We train a StableSyncNet on VoxCeleb2 [10] and test it on HDTF [51], which is an out-of-distribution experimental setup. The validation loss on VoxCeleb2 reaches around 0.18 and the accuracy on HDTF achieves 94%, which significantly surpasses the previous SOTA result 91% [16, 29].

5. Experiments

5.1. Experimental Settings

Datasets. We used a mixture of VoxCeleb2 [10] and HDTF [51] datasets as our training set. VoxCeleb2 is a large-scale audio-visual dataset containing over 1 million utterances from over 6,000 speakers. It includes speakers from a wide range of ethnicities, accents, and backgrounds. HDTF contains 362 different high-definition (HD) videos, with resolutions typically around 720p to 1080p.

Method	HDTF					VoxCeleb2				
	FID ↓	SSIM ↑	Sync _{conf} ↑	LMD ↓	FVD ↓	FID ↓	SSIM ↑	Sync _{conf} ↑	LMD ↓	FVD ↓
Wav2Lip [29]	12.5	0.70	8.2	0.34	304.35	10.8	0.71	7.0	0.53	257.85
VideoReTalking [8]	9.5	0.75	7.5	0.49	270.56	7.5	0.77	6.4	0.60	215.67
Diff2Lip [28]	10.3	0.72	7.9	0.36	260.45	9.8	0.73	6.9	0.54	210.45
MuseTalk [50]	9.35	0.74	6.8	0.56	246.75	7.1	0.80	5.9	0.64	203.43
LatentSync (Ours)	7.22	0.79	8.9	0.30	162.74	5.7	0.81	7.3	0.51	123.27

Table 1. Quantitative comparisons on HDTF and VoxCeleb2.



Figure 11. Qualitative comparisons with SOTA lip-sync methods. We run two cases in the cross generation setting [28]. The first row demonstrates the original input video, and the second row is the video from which we extracted the audio as input, the video can be regarded as the target lip movements. Rows 3 ~ 7 display the lip-synced videos. (All the photorealistic portrait images in this paper are from contracted models.)

We used HyperIQA [40] to filter out videos with low visual quality, specifically blurry or pixelated videos. During evaluation, we randomly selected 30 videos from the test set of HDTF or VoxCeleb2.

Implementation details. When evaluating our model LatentSync, we first converted the videos to 25 FPS, then applied the affine transformation based on facial landmarks detected by face-alignment [5] to obtain 256×256 face videos. The audio was resampled to 16kHz. We used 20 steps of DDIM [38] sampling for inference.

Evaluation metrics. We evaluate our method in three as-

pects: (1) Visual quality. We use SSIM [45] in the reconstruction setting and FID [18] in the cross generation setting to assess visual quality. Following [28], the reconstruction setting refers to using the same audio as the input video, while the cross generation setting refers to using audio different from the input video. (2) Lip-sync accuracy. We use the confidence score of SyncNet (Sync_{conf}) [9] and the landmark distances around the mouth (LMD) [14]. We found that Sync_{conf} aligns closely with visual assessments. (3) Temporal consistency. We adopt the widely used FVD metric [42].

Method	Sync _{conf} ↑	FVD ↓
LatentSync w/o SyncNet	4.6	220.37
LatentSync + latent space SyncNet	7.9	180.45
LatentSync + pixel space SyncNet	8.9	162.74

Table 2. The ablation studies of different SyncNets. HDTF results.

5.2. Comparisons

Comparison methods. We selected several SOTA methods that provide open-source inference code and checkpoints for comparison. Wav2Lip [29] is the classic lip-sync method, introducing the idea of using a pretrained SyncNet for supervision instead of a lip-sync discriminator [24]. VideoReTalking [8] divides the lip-sync process into three steps to improve the results. Diff2Lip [28] utilized pixel-space diffusion models to achieve generalized lip sync. MuseTalk [50] utilizes the architecture of Stable Diffusion for inpainting, but it is not based on the diffusion model framework and appears more like a GAN-based approach.

Quantitative comparisons. As shown in Tab. 1, the lip-sync accuracy of our method significantly surpasses that of other methods. This is attributed to our 94% accuracy StableSyncNet, as well as the audio cross-attention layers in U-Net, which better captures the relationship between audio and lip movements. In terms of visual quality, our method outperforms others, likely due to the powerful capabilities of the Stable Diffusion model. Owing to temporal layer [15] and the incorporation of TREPA, our FVD score is also superior to other methods.

Qualitative comparisons. We run two cases in the cross generation setting. According to Fig. 11, Wav2Lip has excellent lip-sync accuracy, but the generated videos are very blurry. VideoReTalking shows strange artifacts. Diff2Lip is limited by pixel-space diffusion models and can only generate low-resolution videos, resulting in noticeable blurriness. MuseTalk does not preserve facial features well, the man’s beard becomes sparse. In contrast, our method excels in both clarity and identity preservation, even the mole on the woman’s face was preserved. Furthermore, it hardly shows generated box due to the smooth shape of fixed mask.

5.3. Ablation studies

The effectiveness of SyncNet supervision. As shown in Tab. 2, when the SyncNet supervision is not added, The lip-sync performance of the trained diffusion models is significantly poor. In fact, we found that other end-to-end lipsync methods [28, 29] exhibit similar phenomena. As for supervision in two different spaces, diffusion models under pixel space SyncNet supervision perform better in terms of lip-sync accuracy and temporal consistency. This is likely due to the poor convergence of latent space SyncNet (as shown

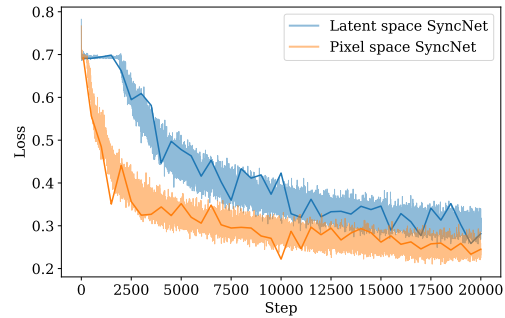


Figure 12. SyncNet training curves of different visual input spaces. Here we use the open-sourced pretrained VAE from Stability AI [1] for encoding. (VoxCeleb2, Batch size 512, StableSyncNet arch, Dim 1024, 16 frames.)

Method	FID ↓	SSIM ↑	FVD ↓
LatentSync	7.71	0.77	176.35
LatentSync + TREPA	7.22	0.79	162.74

Table 3. The ablation studies of TREPA. HDTF results.

in Fig. 12), which is reasonable since the input to the latent space SyncNet is the compressed latents obtained from VAE encoding, and some lip information may already be lost.

In addition, we found that improvements in lip-sync accuracy were accompanied by an increase in temporal consistency. This is because the audio window inherently encapsulates rich temporal information. Enhanced utilization of audio information by the model also leads to the improved temporal consistency.

The effectiveness of TREPA. According to Tab. 3, both the temporal consistency and visual quality improve after incorporating TREPA. This improvement may be attributed to that the robust representations extracted by VideoMAE-v2 [44] inherently encapsulate both visual and temporal information.

6. Conclusion

We introduced LatentSync, the first lip-sync method based on audio-conditioned LDMs, which addresses the problems of traditional diffusion-based lip-sync methods: (1) The low sampling speed and inability to generate high-resolution videos of pixel space diffusion. (2) The information loss in two-stage generation methods. We identified the shortcut learning problem in lip-sync task and explored different approaches to incorporate SyncNet supervision to solve this problem. We conducted comprehensive ablation studies to find out several key factors influencing SyncNet converge. In addition, we proposed TREPA to further improve the temporal consistency of our method.

References

- [1] Stability AI. sd-vae-ft-mse. <https://huggingface.co/stabilityai/sd-vae-ft-mse>, 2022. 8
- [2] Martin Arjovsky, Soumith Chintala, and Léon Bottou. Wasserstein generative adversarial networks. In *International conference on machine learning*, pages 214–223. PMLR, 2017. 1
- [3] Dan Bigioi, Shubhajit Basak, Michał Stypułkowski, Maciej Zieba, Hugh Jordan, Rachel McDonnell, and Peter Corcoran. Speech driven video editing via an audio-conditioned diffusion model. *Image and Vision Computing*, 142:104911, 2024. 1, 2
- [4] Andreas Blattmann, Robin Rombach, Huan Ling, Tim Dockhorn, Seung Wook Kim, Sanja Fidler, and Karsten Kreis. Align your latents: High-resolution video synthesis with latent diffusion models. In *Proceedings of the IEEE/CVF Conference on Computer Vision and Pattern Recognition*, pages 22563–22575, 2023. 4
- [5] Adrian Bulat and Georgios Tzimiropoulos. How far are we from solving the 2d & 3d face alignment problem?(and a dataset of 230,000 3d facial landmarks). In *Proceedings of the IEEE international conference on computer vision*, pages 1021–1030, 2017. 4, 7
- [6] Tong Che, Yanran Li, Athul Paul Jacob, Yoshua Bengio, and Wenjie Li. Mode regularized generative adversarial networks. *arXiv preprint arXiv:1612.02136*, 2016. 1
- [7] Zhiyuan Chen, Jiajiong Cao, Zhiquan Chen, Yuming Li, and Chenguang Ma. Echomimic: Lifelike audio-driven portrait animations through editable landmark conditions. *arXiv preprint arXiv:2407.08136*, 2024. 2, 3
- [8] Kun Cheng, Xiaodong Cun, Yong Zhang, Menghan Xia, Fei Yin, Mingrui Zhu, Xuan Wang, Jue Wang, and Nannan Wang. Videoretalking: Audio-based lip synchronization for talking head video editing in the wild. In *SIGGRAPH Asia 2022 Conference Papers*, pages 1–9, 2022. 3, 5, 7, 8
- [9] Joon Son Chung and Andrew Zisserman. Out of time: automated lip sync in the wild. In *Computer Vision–ACCV 2016 Workshops: ACCV 2016 International Workshops, Taipei, Taiwan, November 20–24, 2016, Revised Selected Papers, Part II 13*, pages 251–263. Springer, 2017. 2, 4, 5, 6, 7, 1
- [10] Joon Son Chung, Arsha Nagrani, and Andrew Zisserman. Voxceleb2: Deep speaker recognition. *arXiv preprint arXiv:1806.05622*, 2018. 6, 1
- [11] Patrick Esser, Robin Rombach, and Bjorn Ommer. Taming transformers for high-resolution image synthesis. In *Proceedings of the IEEE/CVF conference on computer vision and pattern recognition*, pages 12873–12883, 2021. 2, 4
- [12] Robert Geirhos, Jörn-Henrik Jacobsen, Claudio Michaelis, Richard Zemel, Wieland Brendel, Matthias Bethge, and Felix A Wichmann. Shortcut learning in deep neural networks. *Nature Machine Intelligence*, 2(11):665–673, 2020. 2
- [13] Ian Goodfellow, Jean Pouget-Abadie, Mehdi Mirza, Bing Xu, David Warde-Farley, Sherjil Ozair, Aaron Courville, and Yoshua Bengio. Generative adversarial nets. *Advances in neural information processing systems*, 27, 2014. 3
- [14] Jiazhi Guan, Zhanwang Zhang, Hang Zhou, Tianshu Hu, Kaisiyuan Wang, Dongliang He, Haocheng Feng, Jingtuo Liu, Errui Ding, Ziwei Liu, et al. Stylesync: High-fidelity generalized and personalized lip sync in style-based generator. In *Proceedings of the IEEE/CVF Conference on Computer Vision and Pattern Recognition*, pages 1505–1515, 2023. 1, 3, 5, 7
- [15] Yuwei Guo, Ceyuan Yang, Anyi Rao, Zhengyang Liang, Yaohui Wang, Yu Qiao, Maneesh Agrawala, Dahua Lin, and Bo Dai. Animatediff: Animate your personalized text-to-image diffusion models without specific tuning. *arXiv preprint arXiv:2307.04725*, 2023. 3, 4, 8
- [16] Anchit Gupta, Rudrabha Mukhopadhyay, Sindhu Balachandra, Faizan Farooq Khan, Vinay P Nambodiri, and CV Jawahar. Towards generating ultra-high resolution talking-face videos with lip synchronization. In *Proceedings of the IEEE/CVF Winter Conference on Applications of Computer Vision*, pages 5209–5218, 2023. 2, 6
- [17] Kaiming He, Xiangyu Zhang, Shaoqing Ren, and Jian Sun. Deep residual learning for image recognition. In *Proceedings of the IEEE conference on computer vision and pattern recognition*, pages 770–778, 2016. 5
- [18] Martin Heusel, Hubert Ramsauer, Thomas Unterthiner, Bernhard Nessler, and Sepp Hochreiter. Gans trained by a two time-scale update rule converge to a local nash equilibrium. *Advances in neural information processing systems*, 30, 2017. 7
- [19] Jonathan Ho, Ajay Jain, and Pieter Abbeel. Denoising diffusion probabilistic models. *Advances in neural information processing systems*, 33:6840–6851, 2020. 4
- [20] Jianwen Jiang, Chao Liang, Jiaqi Yang, Gaojie Lin, Tianyun Zhong, and Yanbo Zheng. Loopy: Taming audio-driven portrait avatar with long-term motion dependency. In *The Thirteenth International Conference on Learning Representations*, 2024. 2, 3
- [21] Minguk Kang, Jun-Yan Zhu, Richard Zhang, Jaesik Park, Eli Shechtman, Sylvain Paris, and Taesung Park. Scaling up gans for text-to-image synthesis. In *Proceedings of the IEEE/CVF Conference on Computer Vision and Pattern Recognition*, pages 10124–10134, 2023. 1
- [22] Tero Karras, Samuli Laine, Miika Aittala, Janne Hellsten, Jaakko Lehtinen, and Timo Aila. Analyzing and improving the image quality of stylegan. In *Proceedings of the IEEE/CVF conference on computer vision and pattern recognition*, pages 8110–8119, 2020. 3
- [23] Diederik P Kingma. Auto-encoding variational bayes. *arXiv preprint arXiv:1312.6114*, 2013. 2, 4
- [24] Prajwal KR, Rudrabha Mukhopadhyay, Jerin Philip, Abhishek Jha, Vinay Nambodiri, and CV Jawahar. Towards automatic face-to-face translation. In *Proceedings of the 27th ACM international conference on multimedia*, pages 1428–1436, 2019. 8
- [25] Tao Liu, Chenpeng Du, Shuai Fan, Feilong Chen, and Kai Yu. Diffdub: Person-generic visual dubbing using inpainting renderer with diffusion auto-encoder. In *ICASSP 2024-2024 IEEE International Conference on Acoustics, Speech and Signal Processing (ICASSP)*, pages 3630–3634. IEEE, 2024. 1, 2

- [26] Camillo Lugaresi, Jiuqiang Tang, Hadon Nash, Chris McClanahan, Esha Uboweja, Michael Hays, Fan Zhang, Chuoling Chang, Ming Guang Yong, Juhyun Lee, et al. Mediapipe: A framework for building perception pipelines. *arXiv preprint arXiv:1906.08172*, 2019. 4
- [27] Yifeng Ma, Shiwei Zhang, Jiayu Wang, Xiang Wang, Yingya Zhang, and Zhidong Deng. Dreamtalk: When expressive talking head generation meets diffusion probabilistic models. *arXiv preprint arXiv:2312.09767*, 2023. 5
- [28] Soumik Mukhopadhyay, Saksham Suri, Ravi Teja Gadde, and Abhinav Shrivastava. Diff2lip: Audio conditioned diffusion models for lip-synchronization. In *Proceedings of the IEEE/CVF Winter Conference on Applications of Computer Vision*, pages 5292–5302, 2024. 1, 2, 5, 7, 8
- [29] KR Prajwal, Rudrabha Mukhopadhyay, Vinay P Namboodiri, and CV Jawahar. A lip sync expert is all you need for speech to lip generation in the wild. In *Proceedings of the 28th ACM international conference on multimedia*, pages 484–492, 2020. 1, 2, 3, 4, 5, 6, 7, 8
- [30] Konpat Preechakul, Nattanat Chatthee, Suttisak Widadwongsa, and Supasorn Suwajanakorn. Diffusion autoencoders: Toward a meaningful and decodable representation. In *Proceedings of the IEEE/CVF conference on computer vision and pattern recognition*, pages 10619–10629, 2022. 2
- [31] primepake. wav2lip 288x288. https://github.com/primepake/wav2lip_288x288, 2021. 6
- [32] Alec Radford, Jong Wook Kim, Tao Xu, Greg Brockman, Christine McLeavey, and Ilya Sutskever. Robust speech recognition via large-scale weak supervision. In *International conference on machine learning*, pages 28492–28518. PMLR, 2023. 3
- [33] Robin Rombach, Andreas Blattmann, Dominik Lorenz, Patrick Esser, and Björn Ommer. High-resolution image synthesis with latent diffusion models. In *Proceedings of the IEEE/CVF conference on computer vision and pattern recognition*, pages 10684–10695, 2022. 2, 3, 5
- [34] Olaf Ronneberger, Philipp Fischer, and Thomas Brox. U-net: Convolutional networks for biomedical image segmentation. In *Medical image computing and computer-assisted intervention—MICCAI 2015: 18th international conference, Munich, Germany, October 5–9, 2015, proceedings, part III 18*, pages 234–241. Springer, 2015. 3
- [35] Tim Salimans, Ian Goodfellow, Wojciech Zaremba, Vicki Cheung, Alec Radford, and Xi Chen. Improved techniques for training gans. *Advances in neural information processing systems*, 29, 2016. 1
- [36] Axel Sauer, Tero Karras, Samuli Laine, Andreas Geiger, and Timo Aila. Stylegan-t: Unlocking the power of gans for fast large-scale text-to-image synthesis. In *International conference on machine learning*, pages 30105–30118. PMLR, 2023. 1
- [37] Karen Simonyan and Andrew Zisserman. Very deep convolutional networks for large-scale image recognition. *arXiv preprint arXiv:1409.1556*, 2014. 4
- [38] Jiaming Song, Chenlin Meng, and Stefano Ermon. Denoising diffusion implicit models. *arXiv preprint arXiv:2010.02502*, 2020. 7
- [39] Akash Srivastava, Lazar Valkov, Chris Russell, Michael U Gutmann, and Charles Sutton. Veegan: Reducing mode collapse in gans using implicit variational learning. *Advances in neural information processing systems*, 30, 2017. 1
- [40] Shaolin Su, Qingsen Yan, Yu Zhu, Cheng Zhang, Xin Ge, Jinqiu Sun, and Yanning Zhang. Blindly assess image quality in the wild guided by a self-adaptive hyper network. In *Proceedings of the IEEE/CVF conference on computer vision and pattern recognition*, pages 3667–3676, 2020. 7
- [41] Linrui Tian, Qi Wang, Bang Zhang, and Liefeng Bo. Emo: Emote portrait alive-generating expressive portrait videos with audio2video diffusion model under weak conditions. *arXiv preprint arXiv:2402.17485*, 2024. 2, 3
- [42] Thomas Unterthiner, Sjoerd Van Steenkiste, Karol Kurach, Raphael Marinier, Marcin Michalski, and Sylvain Gelly. Towards accurate generative models of video: A new metric & challenges. *arXiv preprint arXiv:1812.01717*, 2018. 7
- [43] A Vaswani. Attention is all you need. *Advances in Neural Information Processing Systems*, 2017. 5
- [44] Limin Wang, Bingkun Huang, Zhiyu Zhao, Zhan Tong, Yinan He, Yi Wang, Yali Wang, and Yu Qiao. Videomae v2: Scaling video masked autoencoders with dual masking. In *Proceedings of the IEEE/CVF Conference on Computer Vision and Pattern Recognition*, pages 14549–14560, 2023. 5, 8
- [45] Zhou Wang, Alan C Bovik, Hamid R Sheikh, and Eero P Simoncelli. Image quality assessment: from error visibility to structural similarity. *IEEE transactions on image processing*, 13(4):600–612, 2004. 7
- [46] Mingwang Xu, Hui Li, Qingkun Su, Hanlin Shang, Liwei Zhang, Ce Liu, Jingdong Wang, Luc Van Gool, Yao Yao, and Siyu Zhu. Hallo: Hierarchical audio-driven visual synthesis for portrait image animation. *arXiv preprint arXiv:2406.08801*, 2024. 2, 3
- [47] Zhenhui Ye, Ziyue Jiang, Yi Ren, Jinglin Liu, Jinzheng He, and Zhou Zhao. Geneface: Generalized and high-fidelity audio-driven 3d talking face synthesis. *arXiv preprint arXiv:2301.13430*, 2023. 5
- [48] Runyi Yu, Tianyu He, Ailing Zeng, Yuchi Wang, Junliang Guo, Xu Tan, Chang Liu, Jie Chen, and Jiang Bian. Make your actor talk: Generalizable and high-fidelity lip sync with motion and appearance disentanglement. *arXiv preprint arXiv:2406.08096*, 2024. 1, 2
- [49] Richard Zhang, Phillip Isola, Alexei A Efros, Eli Shechtman, and Oliver Wang. The unreasonable effectiveness of deep features as a perceptual metric. In *Proceedings of the IEEE conference on computer vision and pattern recognition*, pages 586–595, 2018. 3, 4
- [50] Yue Zhang, Minhao Liu, Zhaokang Chen, Bin Wu, Yubin Zeng, Chao Zhan, Yingjie He, Junxin Huang, and Wenjiang Zhou. Musetalk: Real-time high quality lip synchronization with latent space inpainting. *arXiv preprint arXiv:2410.10122*, 2024. 3, 5, 7, 8
- [51] Zhimeng Zhang, Lincheng Li, Yu Ding, and Changjie Fan. Flow-guided one-shot talking face generation with a high-resolution audio-visual dataset. In *Proceedings of the IEEE/CVF Conference on Computer Vision and Pattern Recognition*, pages 3661–3670, 2021. 2, 6

- [52] Zhimeng Zhang, Zhipeng Hu, Wenjin Deng, Changjie Fan, Tangjie Lv, and Yu Ding. Dinet: Deformation inpainting network for realistic face visually dubbing on high resolution video. In *Proceedings of the AAAI Conference on Artificial Intelligence*, pages 3543–3551, 2023. [1](#), [3](#), [5](#)
- [53] Weizhi Zhong, Jichang Li, Yinqi Cai, Liang Lin, and Guanbin Li. Style-preserving lip sync via audio-aware style reference. *arXiv preprint arXiv:2408.05412*, 2024. [1](#), [2](#)

Appendix

A. SyncNet Training Loss Proof

According to the classic training framework of SyncNet [9, 29], we randomly provide SyncNet with positive and negative samples with a 50% probability during the training stage. The output of SyncNet is a probability distribution of whether the sample is positive or negative. We define $p(x = 1)$ as the probability that the sample is positive, and $p(x = 0)$ as the probability that the sample is negative. Let $p(x)$ be the true probability distribution and $q(x)$ the predicted probability distribution. We plot some scatter charts to observe the changes in the prediction probabilities of a non-converging SyncNet during the training process.

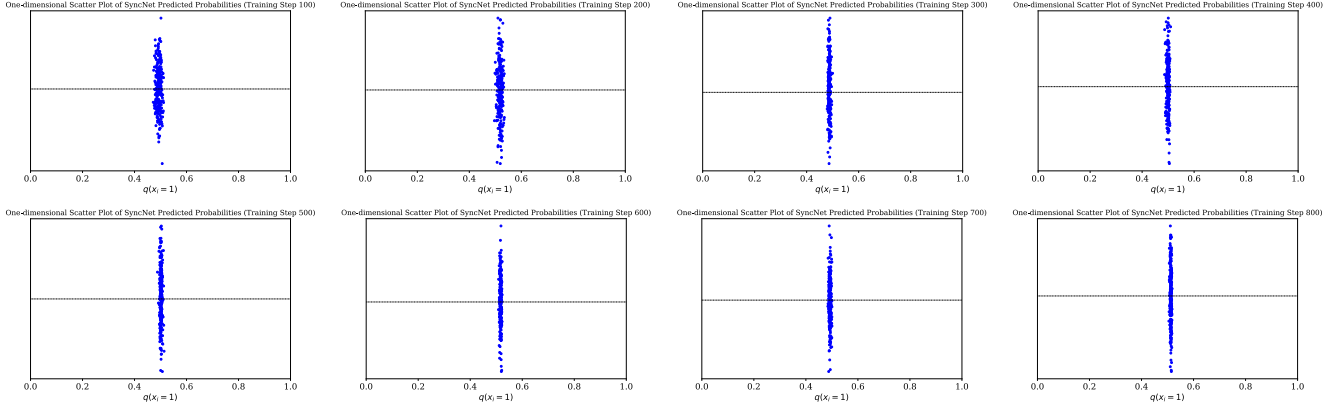


Figure 13. We train a SyncNet on VoxCeleb2 [10] with batch size of 256. We modify its architecture and data to make it non-converging. Every 100 steps, we plot a scatter plot to observe the probability distribution of SyncNet’s predicted $q(x_i = 1)$, including 256 data points. The x-axis represents the probability $q(x_i = 1)$, and we add some random jitter along the y-axis for better visualization.

As shown in Fig. 13, in the early stages of training, the probabilities predicted by SyncNet for $q(x_i = 1)$ are dispersed, but later in the training, the probabilities for $q(x_i = 1)$ are almost all distributed around 0.5 (the scatter charts for $q(x_i = 0)$ are similar). Now we have:

$$\forall i \in 1, 2, \dots, N : q(x_i = 1) \approx q(x_i = 0) \approx 0.5 \quad (8)$$

We speculate that this may be because, the non-converging SyncNet is consistently unable to correctly distinguish whether a sample is positive or negative during the training process. However, to reduce the training loss, it tends to output a probability of 0.5 for all input embeddings to minimize the training loss as much as possible. This is why the training loss decreases somewhat initially and then gets stuck (from 0.8 to 0.69).

We assume that there are A positive samples and B negative samples in a batch, and then we can derive SyncNet’s training loss based on the following steps:

$$\mathcal{L}_{\text{syncnet}} = -\frac{1}{N} \sum_{i=1}^N \sum_{x_i \in \{0,1\}} p(x_i) \log q(x_i) \quad (9)$$

$$= -\frac{1}{N} \sum_{i=1}^N [p(x_i = 1) \log q(x_i = 1) + p(x_i = 0) \log q(x_i = 0)] \quad (10)$$

$$= -\frac{1}{N} \sum_{i=1}^N p(x_i = 1) \log q(x_i = 1) - \frac{1}{N} \sum_{i=1}^N p(x_i = 0) \log q(x_i = 0) \quad (11)$$

$$= -\frac{1}{N} \left[\sum_{a=1}^A 1 \times \log q(x_a = 1) + \sum_{b=1}^B 0 \times \log q(x_b = 1) \right] - \frac{1}{N} \left[\sum_{a=1}^A 0 \times \log q(x_a = 1) + \sum_{b=1}^B 1 \times \log q(x_b = 1) \right] \quad (12)$$

$$= -\frac{1}{N} \left[\sum_{a=1}^A \log q(x_a = 1) + \sum_{b=1}^B \log q(x_b = 0) \right] \quad (13)$$

$$\approx -\frac{1}{N} [A \log 0.5 + B \log 0.5] \quad \text{Apply Eq. (8)} \quad (14)$$

$$= 0.693 \quad (15)$$